PAGEOPH, Vol. 143, No. 1/2/3 (1994)

0033–4553/94/030425–32$1.50 + 0.20/0

Laboratory Measurement of Compaction-induced Permeability Change in Porous Rocks: Implications for the Generation and Maintenance of Pore Pressure Excess in the Crust

CHRISTIAN DAVID,[1,2] TENG-FONG WONG,[1] WENLU ZHU[1] and JIAXIANG ZHANG[1,3]

Abstract—Permeability exerts significant control over the development of pore pressure excess in the crust, and it is a physical quantity sensitively dependent on the pore structure and stress state. In many applications, the relation between permeability and effective mean stress is assumed to be exponential and that between permeability and porosity is assumed to be a power law, so that the pressure sensitivity of permeability is characterized by the coefficient γ and the porosity sensitivity by the exponent α. In this study, we investigate experimentally the dependence of permeability on pressure and porosity in five sandstones with porosities ranging from 14% to 35% and we review published experimental data on intact rocks, unconsolidated materials and rock fractures. The laboratory data show that the pressure and porosity sensitivities differ significantly for different compaction mechanisms, but for a given compaction mechanism, the data can often be approximated by the empirical relations. The permeabilities of tight rocks and rock joints show relatively high pressure sensitivity and low porosity sensitivity. A wide range of values for α and γ have been observed in relation to the mechanical compaction of porous rocks, sand and fault gouge, whereas the porosity sensitivity for chemical compaction processes is often observed to be given by $\alpha \approx 3$. We show that since the ratio γ/α corresponds to the pore compressibility, the different dependences of permeability on porosity and pressure are related to the pore structure and its compressibility. Guided by the laboratory data, we conduct numerical simulations on the development of pore pressure in crustal tectonic settings according to the models of WALDER and NUR (1984) and RICE (1992). Laboratory data suggest that the pressure sensitivity of fault gouge is relatively low, and to maintain pore pressure at close to the lithostatic value in the Rice model, a relatively high influx of fluid from below the seismogenic layer is necessary. The fluid may be injected as vertically propagating pressure pulses into the seismogenic system, and RICE's (1992) critical condition for the existence of solitary wave is shown to be equivalent to $\alpha > 1$, which is satisfied by most geologic materials in the laboratory. Laboratory data suggest that the porosity sensitivity is relatively high when the permeability is reduced by a coupled mechanical and chemical compaction process. This implies that in a crustal layer, pore pressure may be generated more efficiently than cases studied by WALDER and NUR (1984) who assumed a relatively low porosity sensitivity of $\alpha = 2$.

Key words: Permeability, compaction, fluid pressure generation, effective pressure, fault mechanics, fault hydraulics.

---

[1] State University of New York at Stony Brook, Department of Earth and Space Sciences, Stony Brook, NY 11794-2100, U.S.A.

[2] Now at: Institut de Physique du Globe, 5 rue René Descartes, F-67084 Strasbourg, France.

[3] Now at: Amoco Production Company, P.O. Box 3385, Tulsa, OK 74102, U.S.A.

Introduction

Fluids exert significant mechanical and chemical effects on virtually all crustal processes. HUBBERT and RUBEY's (1959) theory of overthrusting underscored the influence of pore pressure on tectonic processes. Numerous mechanisms for the generation and the maintenance of high pore pressure in sedimentary, metamorphic, and tectonic processes have been identified (e.g., BREDEHOEFT and HANSHAW, 1968), and their consequences in seismotectonics, economic geology, petroleum geology, aqueous geochemistry, and geotechnical engineering have been extensively investigated (see recent reviews edited by BREDEHOEFT and NORTON (1990) and by TORGERSEN (1991).

To model the fluid percolation process for a specific tectonic and lithological setting, one of the most difficult problems has been the estimation of the permeability, a quantity which varies by more than 10 orders of magnitude in common geological materials (FREEZE and CHERRY, 1979). The problem is complicated by the fact that the *in situ* permeability values can be significantly higher than the laboratory values due to enhanced flow in mesoscopic scale fractures (BRACE, 1980). A wide range of pressure and temperature conditions are also encountered in tectonic and metamorphic processes (FYFE *et al.*, 1978) and this variation in pressure and temperature may influence the permeability significantly. Since it is difficult to come up with even an order-of-magnitude estimate, the permeability in a given formation is often idealized in theoretical models as not changing temporally or spatially (e.g., BREDEHOEFT and HANSHAW, 1968; BRACE, 1980).

A number of recent observations indicate that the pore pressures in many seismotectonic settings are relatively high. Heat flow, *in situ* stress and seismological measurements (e.g., ZOBACK *et al.*, 1987; LACHENBRUCH and SASS, 1992) suggest that the San Andreas fault is mechanically weak in an absolute sense as well as in a relative sense. These low stress values are in accordance with laboratory measurements of the frictional strength (Byerlee's law) only if anomalously high pore pressure exists in a mature fault zone such as the San Andreas (BYERLEE, 1990; RICE, 1992). In subduction zones and convergent margins, Ocean Drilling Project (ODP) data indicate that overpressure is common in and below a number of accretionary wedges (e.g., MOORE, 1989; BANGS *et al.*, 1990; VROLIJK *et al.* 1988). As large volumes of fluids are generated during offscraping and underthrusting they migrate through the prism, transferring heat and forming zones of abnormal pore pressures. High pore pressures influence the mechanical deformation and failure mode at all scales (DAVIS *et al.*, 1983; BYRNE and FISHER, 1990; KARIG, 1990). In many low- to medium-grade metamorphic settings, geological observations of extensive crack sealing and healing activity imply the existence of free water, possibly at pressures significantly higher than hydrostatic (ETHERIDGE *et al.*, 1984; WALDER and NUR, 1984).

The overpressure can be generated and maintained over a relatively long time only if the permeability is low and if there exists a physical mechanism corresponding to a "source term" in the hydraulic diffusion equation. For example, RICE (1992) appealed to the continuous influx of fluid from the "ductile root" of the fault zone to maintain the super-hydrostatic pore pressure in his recent model for the pore pressure and stress states of the San Andreas fault. WALDER and NUR (1984) appealed to continual porosity reduction by crack healing and sealing processes to generate a nearly lithostatic pressure which would then be relieved by hydraulic fracturing in their model for the cyclic hydraulics in the crust.

For overpressure to develop in these models, it is necessary for permeability to be a variable sensitively dependent on porosity change and stress. Motivated by the data of BERNABÉ *et al.* (1982) on synthetic samples of hot-pressed calcite, WALDER and NUR (1984) postulated that permeability decreases with porosity reduction according to a power law. Motivated by laboratory (BRACE *et al.*, 1968) and *in situ* (PRATT *et al.*, 1977) measurements on granite, RICE (1992) assumed an exponential decay of permeability with effective pressure. To what extent are such empirical relations applicable to various rock types under crustal conditions? How are the two different formulations related to one another? Can any connections be made between such phenomenological formulations and micromechanical models (e.g., WALSH, 1981)? To address these questions, it is desirable to have a comprehensive database characterizing the dependences of permeability and porosity on the (hydrostatic and deviatoric) stresses, pore pressure, lithology, rock fabric and deformation mechanism.

We present in this paper new laboratory measurements of permeability of porous sandstones compacted under hydrostatic stresses. We are particularly interested in the question: how does the compaction mechanism influence the relation among permeability, porosity and effective pressure? Our data should be useful for modeling not only sedimentary processes, but also overpressure processes in fault zones and accretionary prisms because in many respects, the weakly cemented sandstones are analogs for granular materials (such as fault gouge and sediments) subjected to analogous compaction processes. We then review existing laboratory data on permeability of sedimentary and crystalline rocks, focusing on the influence of compaction mechanism. In particular we address the question: to what extent do the published data on intact and fractured rocks as well as fault gouge agree with the power law (WALDER and NUR, 1984) and exponential relation (RICE, 1992) for permeability? Are parameters chosen for previous theoretical studies representative of typical values measured in the laboratory, and if not, what are the implications on the generation and maintenance of pore pressure excess in crustal tectonic settings? Guided by the laboratory data, we address these questions by conducting a series of numerical simulations using an appropriately wide range of parameters for the development of pore pressure excess in a seismogenic system and in a crustal layer undergoing inelastic porosity reduction.

Experimental Procedure

Measurement of Permeability, Porosity Change and Acoustic Emission

Mechanical compaction tests were conducted following the procedures described in detail by ZHANG *et al.* (1990a). The samples (18.4 mm in diameter and 38.1 mm in length) were saturated with distilled water. The capability of our pressure vessel is 700 MPa, and a Heise gauge was used to measure the confining pressure with an accuracy of 0.5 MPa. The pore pressure is limited to 200 MPa, and it was measured by a strain gage pressure transducer with an accuracy of 0.125 MPa. In this study, all tests were performed at a nominal pore pressure of 10 MPa and at room temperature. Our data will be reported in terms of the difference between the confining and pore pressures, which we will refer to as the "effective pressure." However it should be noted that both theoretical (WALSH, 1981) and experimental (BERNABÉ, 1987; DAVID and DAROT, 1989; ZOBACK and BYERLEE, 1975) results have shown that the confining pressure and pore pressure may have somewhat different effects on permeability. We have not determined yet the exact form of the effective pressure law for our sandstones.

The porosity change was calculated from the pore volume change measured with a volumometer as the amount of fluid added to or taken out of the sample to maintain constant pore pressure throughout the experiment. The uncertainty in porosity change was estimated to be $\pm 0.1\%$. We also recorded the acoustic emission activity during the compaction process. This technique has been described in detail by ZHANG *et al.* (1990b). Acoustic emissions are associated with brittle fracture events at the grain scale, either crack nucleation or crack propagation.

The triaxial system was modified to incorporate a wide-range permeameter to measure the permeability under hydrostatic or triaxial conditions. Technical details of the equipment have been described by ZHANG *et al.* (1993). The permeameter can resolve over 8 orders of magnitude in permeability ranging from 5×10^{-12} m^2 (5 D) down to about 10^{-20} m^2 (10 nD). In the high-permeability range, the steady-state flow method was used. The fluid flow rate was measured by monitoring the time interval required for a given amount of water to flow out of the jacketed sample while it was subjected to a constant confining pressure in the vessel. This flow volume was recorded from the increase of the water height in a graduated pipette connected to the downstream pore pressure system of the permeameter. A constant differential pore pressure across the rock sample was maintained by the fine adjustment of a metering valve, and the sample permeability was determined from Darcy's law. In the low-permeability range ($< 10\ \mu$D), we used the transient pulse method (BRACE *et al.*, 1968). The exponential decay in time of the differential pressure across the sample was monitored as a pressure pulse diffused through the sample, and the permeability was inferred from the slope of the decay curve plotted on semi-logarithmic paper. We estimate the uncertainty in permeability measure-

ments to be less than a factor of 2. The permeability of the rock samples was measured at different stages corresponding to increasing values of the confining pressure, starting from an effective pressure of 3 MPa (to ensure that the jacket fitted tightly against the sample). As we lost the information on the compaction behavior when we increased both confining (up to 13 MPa) and pore pressure (up to 10 MPa), our initial conditions are defined at this first pressure step.

Description of the Rock Samples

We have done experiments on five different sandstones with porosities in a wide range (between 14% and 35%). The hydrostatic compaction data for Berea and Boise sandstones have already been presented (ZHANG *et al.*, 1990a), but not the permeability data. New hydromechanical data were obtained for two sandstones (Adamswiller and Rothbach) from the Vosges mountains in eastern France, and for the Fontainebleau sandstone from the Ile-de-France region south of Paris. A petrophysical description of the sandstones, including porosity, grain size and the modal analysis, is given in Table 1. Porosity was calculated from the difference in weight between the water-saturated and dry samples, and the mean grain size has been inferred from chord length analysis on two-dimensional thin sections (ZHANG *et al.*, 1990a). Both the Fontainebleau and Boise sandstones are relatively clay-free.

Table 1

Petrophysical description of the tested sandstones

	Porosity (Φ)	Grain size (radius R)	Critical pressure (P_{cr})	Modal analysis
Adamswiller	22.6%	60 μm	190 MPa	71% quartz 9% felspar 5% oxydes, mica clay content = 11%
Rothbach	19.9%	152 μm	240 MPa	68% quartz 16% felspar 3% oxydes, mica clay content = 12%
Fontainebleau	13.6%	125 μm	350 MPa	99% quartz clay-free
Berea	21.0%	130 μm	380 MPa	71% quartz 10% felspar 5% calcite clay content = 10%
Boise	35.0%	460 μm	75 MPa	40% quartz 50% felspar 5% biotite clay-free

The former has a well-sorted grain-size distribution whereas the latter is characterized by a large mean grain and pore size. All the other sandstones have a significant clay content (above 10% in weight).

Compaction-induced Permeability Change in Sandstones

It is important to distinguish between the fundamentally different behavior of low porosity rock (say $\Phi < 5\%$) and that of very porous rocks (such as sandstones and fault gouge with $\Phi > 15\%$). In low porosity rocks, hydrostatic compaction is nonlinear and reversible, reflecting the elastic closure and opening of microcracks. The effects of microcracks on hydrostatic compaction and permeability evolution have been intensively studied in the past two decades (e.g., BRACE, 1978a,b; BERNABÉ, 1986; TRIMMER *et al.*, 1980). Although the porosity reduction may be as small as 1%, the closing of numerous microcracks in Westerly granite can lower the permeability by as much as two orders of magnitude (BRACE *et al.*, 1968).

In sedimentary geology, most of the previous studies of hydrostatic compaction for porous rocks focus on a relatively narrow pressure range, which corresponds to the range of interest for petroleum engineering purposes. The permeability reduction for such porous materials is in general small compared to that of low porosity rocks (e.g., COYNER, 1984). The porosity reduction resulting from hydrostatic compaction is dominated by grain rearrangement and grain translation processes. Over a sufficiently wide pressure range, the typical hydrostatic compaction curve for porous rocks has a sigmoidal shape, with an inflection point at a given pressure called hereafter the "critical pressure" P_{cr}. This critical pressure corresponds to the onset of grain crushing and pore collapse (BRACE, 1978a). ZHANG *et al.* (1990a) investigated the hydrostatic compaction behavior in five porous sandstones, focusing on the micromechanisms of deformation. The main result was that the critical effective pressure P_{cr} at the onset of pore collapse decreases with increasing porosity (Φ) and increasing grain size (R). As a matter of fact, the Hertzian fracture mechanics model formulated by ZHANG *et al.* (1990a) predicts that P_{cr} scales as $(\phi R)^{-3/2}$, and laboratory data show a good agreement in a wide range of effective pressures over which pore collapse occurs.

The permeability evolution is expected to be significantly different for the three kinds of mechanisms described above. To illustrate this point, we plot in Figure 1 the general trend for permeability variation in low porosity crystalline rocks (Type I behavior), porous sedimentary rocks (Type II), and porous materials compacted at effective stresses beyond critical pressure (Type III), with the deformation mechanism dominated respectively by crack closure, grain rearrangement, and pore collapse. As the range of permeability is the same on both plots in Figure 1 (the scale was only shifted towards lower values on the right-hand side), one can see that the compaction-induced permeability reduction is very effective by microcrack

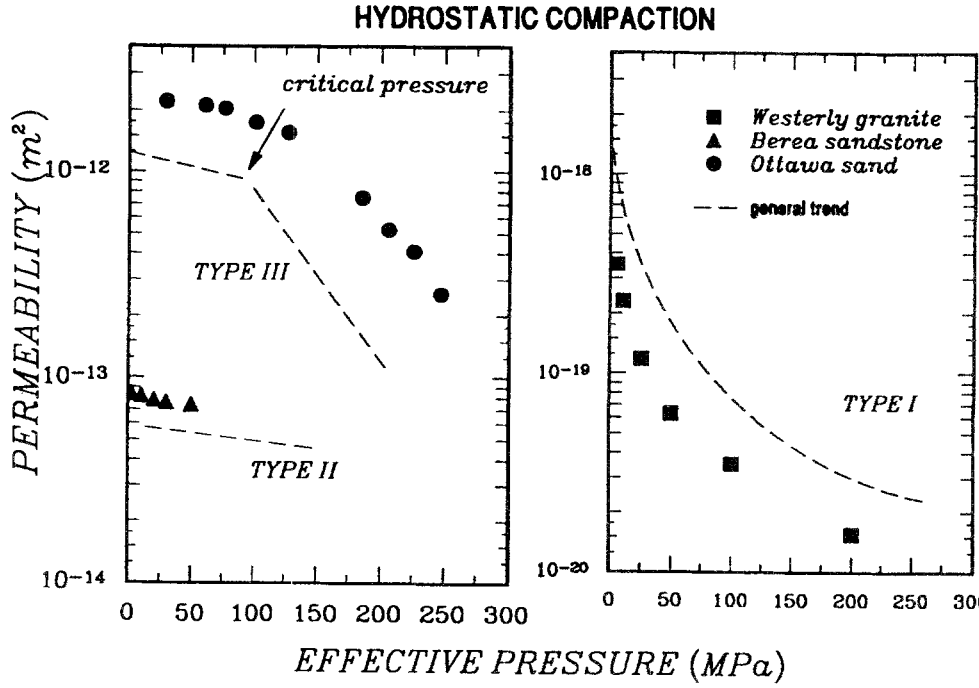

Figure 1

Permeability as a function of effective pressure for three different mechanisms of compaction. Type I is typically observed in a low porosity crystalline rock (such as Westerly granite). The compaction is related to the elastic closure of microcracks, and the pressure sensitivity of permeability decreases with increasing pressure. Type II is typically observed in a porous clastic rock (such as Berea sandstone) for which the compaction is related to the relative movement of grains. The pressure sensitivity of permeability is relatively low. Type III is typically observed in an unconsolidated material (such as Ottawa sand), and it is also observed in porous rocks subjected to elevated pressures. There are two different regimes of compaction, corresponding to relative grain movement (similar to Type II) and grain crushing at elevated pressures. The pressure sensitivity of permeability of the latter is significantly higher than the former.

closure, relatively sluggish for sedimentary rocks, and accelerated in the case of Type III compaction as soon as the critical effective pressure has been reached.

Hydrostatic Compaction and Pore Collapse

Figure 2a shows the hydrostats (effective pressure plotted as a function of porosity reduction) for our five sandstones. On the x axis, the porosity reduction is the pore volume variation normalized to the initial bulk volume of the sample. As discussed before, the reference state corresponds to the first pressure step at 3 MPa effective pressure. The shape of the curves is similar to that found by ZHANG *et al.* (1990a), and the value of the critical pressure can be estimated with good accuracy

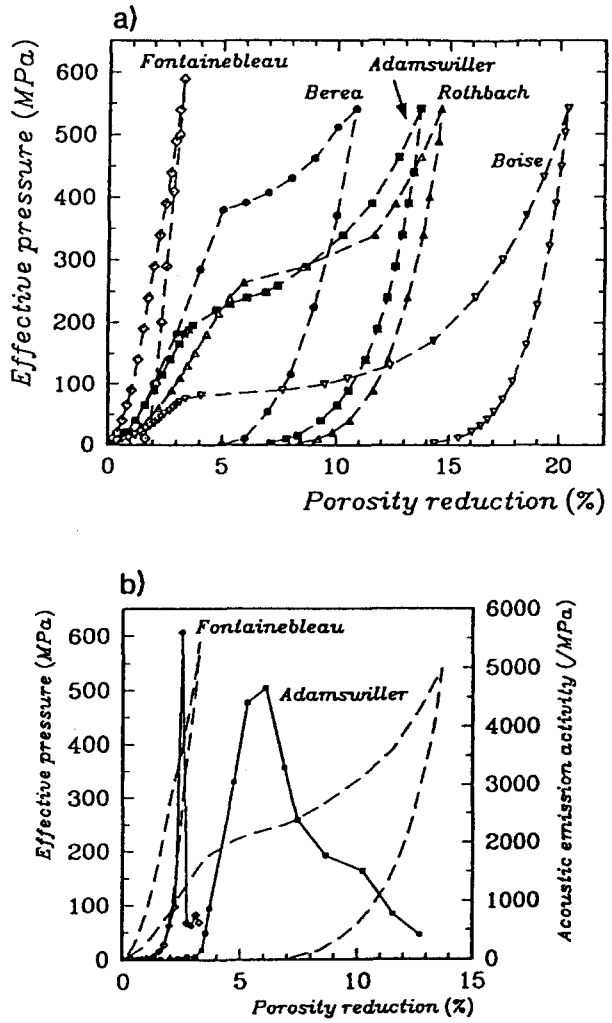

Figure 2

(a) Hydrostats of 5 sandstones. Except for the Fontainebleau sandstone, each of the hydrostats show a sharp inflection point which corresponds to the critical effective pressure for the onset of grain crushing and pore collapse. (b) Effective pressure and acoustic emission (AE) rate as functions of porosity reduction. The onset of grain crushing is marked by a surge of AE activity. Note that the AE activity of the Fontainebleau clearly indicates the onset of grain crushing even though an inflection point was not obvious in the hydrostat.

from the inflection on the hydrostat, and more precisely from the acoustic emission (AE) data since a clear surge in AE activity was observed at the onset of grain crushing. Two sets of data are presented in Figure 2b for Fontainebleau sandstone and Adamswiller sandstone. Fontainebleau sandstone showed an inflection at an effective pressure of 350 MPa, but it can hardly be seen on the scale of Figure 2b.

This is confirmed, however, by the sharp peak in AE at this pressure. The shape of the AE plot for Adamswiller sandstone is much broader: our interpretation is that as this sandstone has an heterogeneous mineralogical content, the grains with different composition fail in a range of effective pressures, unlike Fontainebleau sandstone which is made of quartz grains exclusively. The critical pressures for our sandstones are listed in Table 1. The agreement between our data and the Hertzian fracture mechanics model of ZHANG *et al.* (1990a) is good, except for Adamswiller sandstone which plots below the general trend. A possible explanation may be the high clay and mica content in this rock: the geometry of grain contacts involving these layered minerals may no longer be approximated by the Hertzian type of contact between spheres as required in the model.

Permeability Evolution with Effective Pressure

In Figure 3, we plotted permeability in millidarcy (10^{-15} m^2) as a function of effective pressure in MPa, in a semi-logarithmic plot. The data are for type-II compaction at effective pressures below the critical pressure. For most of our sandstones, a linear trend was observed except for Adamswiller sandstone and for Rothbach sandstone in the very low pressure range during which a significantly higher pressure sensitivity (probably related to microcrack closure) was observed. This means that the compaction-induced permeability reduction can be approximated by an exponential function:

$$K = K_0 \exp[-\gamma(P_{\text{eff}} - P_0)] \tag{1}$$

where K is the permeability at the effective pressure P_{eff}, and K_0 is the permeability at the reference effective pressure P_0, taken to be the atmospheric pressure 0.1 MPa in this study. High values for the pressure sensitivity coefficient γ correspond to a sharper decrease in permeability with P_{eff}. RIEPE *et al.* (1983) and DEBSCHUTZ *et al.* (1989) have previously shown that this empirical relation is suitable for sandstones, and RICE (1992) modeled the development of close to lithostatic pore pressure in the San Andreas fault system assuming such an exponential relation. The type-II compaction data for our sandstones agree reasonably well with this exponential law in the pressure range below the grain crushing regime. The values of K_0 and γ that we calculated are listed in Table 2. Our measurements of the pressure sensitivity coefficient are at least an order of magnitude lower than RICE's (1992) value ($\gamma = 0.2$/MPa).

Our data do not show any clear correlation between γ and petrophysical quantities like porosity or grain size. It is well-known that for a single pore channel embedded in a solid deformed elastically, the pressure sensitivity is much larger for crack-like pores compared to equant pore channels (e.g., WALSH, 1965), so that we expect the permeability variation with pressure to be controlled by the pore shape distribution rather than by bulk parameters like porosity.

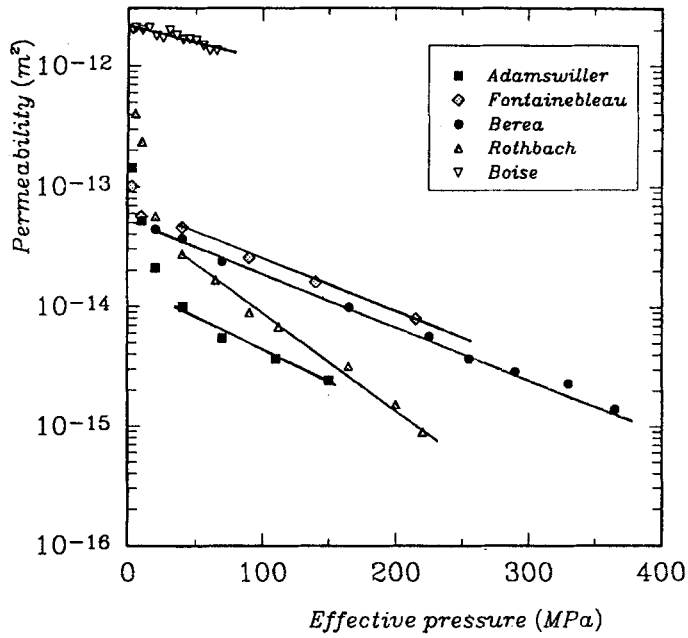

Figure 3
Permeability as a function of effective pressure in 5 sandstones. Except for the Boise, there was a sharp drop in permeability during initial pressurization in each sandstone, probably related to microcrack closure. The subsequent compaction was by relative grain movement, and the permeability evolution with effective pressure followed an approximately exponential trend.

Table 2

Effective pressure sensitivity coefficient and porosity sensitivity exponent for the tested sandstones

	$K = K_0 \exp(-\gamma \cdot P_{eff})$		$K = K_0(\Phi/\Phi_0)^\alpha$	
	$\gamma(\mathrm{MPa}^{-1})$	$K_0(10^{-15}\,\mathrm{m}^2)$	α	$\Phi_0(\%)$
Adamswiller	$12.4\ 10^{-3}$	14.8	25.4	20.7
Fontainebleau	$9.81\ 10^{-3}$	64.8	20.1	13.8
Berea	$9.90\ 10^{-3}$	51.5	14.7	20.4
Rothbach	$18.1\ 10^{-3}$	53.5	18.2	17.7
Boise	$6.62\ 10^{-3}$	2166	4.6	34.9

Permeability Evolution with Porosity

In Figure 4, the same permeability data are plotted as a function of bulk porosity, in a log-log plot. As in Figure 3, a linear correlation has been found for all our sandstones. Therefore, the permeability scales as a powerlaw with porosity:

$$K = K_0(\Phi/\Phi_0)^\alpha \tag{2}$$

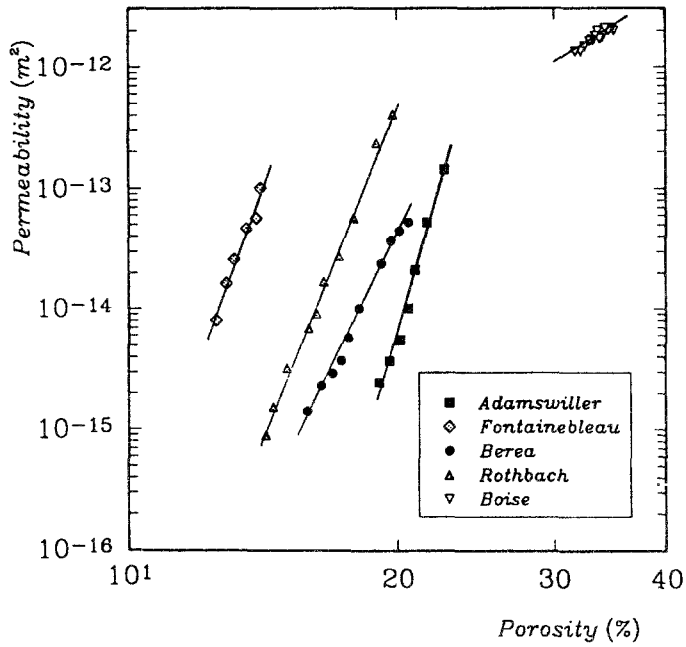

Figure 4
Permeability as a function of porosity in 5 sandstones. The data show reasonable agreement with a power law.

where Φ and Φ_0 are porosity values corresponding to the permeabilities K and K_0, respectively. Figure 4 shows that a rather large permeability loss corresponds to a moderate porosity reduction as pressure is increased, and this results in high values for the porosity sensitivity exponent α. These exponents are listed in Table 2. As for the pressure dependence, there is not a clear correlation with petrophysical properties. Only for Boiše sandstone which has the largest porosity and grain size, we have simultaneously the lowest slope on the permeability-pressure plot, and the smallest value for the exponent α. The most striking result however is the very high values for the exponents: they range from 4.6 for Boise sandstone up to 25 for Adamswiller sandstone. In contrast, recent theoretical models appeal for a considerably weaker dependence of permeability on porosity: for example, WALDER and NUR (1984) chose an exponent $\alpha = 2$ in their model.

Permeability Evolution with Pore Collapse and Grain Crushing

With the exception of Fontainebleau sandstone, we investigated the permeability evolution with type-III compaction at hydrostatic pressures above the critical pressure. We followed the same experimental procedure as described before, but once yielding took place, we had to deal with time-dependent deformation (com-

paction creep) possibly induced by subcritical cracking at constant pressure (ZHANG *et al.*, 1990b). Therefore, one must wait for up to several hours before the rock reaches an equilibrium state before the variation of pore volume and permeability measurement can be conducted.

In Figures 5 and 6 (which are equivalents of Figures 3 and 4 but over a wider range of pressures), we plot in dashed lines the results already shown in Figures 3 and 4 and in solid lines the data corresponding to the pressure range above the critical pressure. The most spectacular evolution was observed for the clay-free Boise sandstone. At the onset of grain crushing, there was a sharp drop in permeability by about three orders of magnitude immediately following the onset of grain crushing at the critical pressure. Permeability switched almost instantaneously from the darcy range into the millidarcy range, and such a dramatic decrease is quite unexpected. Boise sandstone is also the one that showed the largest loss in porosity at the critical pressure (Figure 2). For Berea sandstone, the permeability drop was about one order of magnitude at the critical pressure. On the other hand, the permeability reduction for Adamswiller sandstone and Rothbach sandstone was

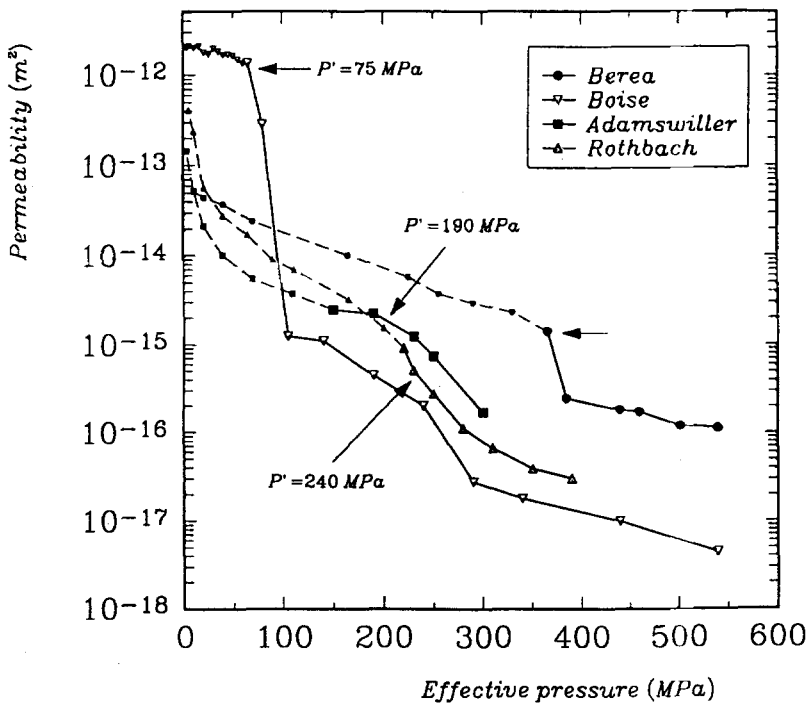

Figure 5

Permeability as a function of effective pressure in 4 sandstones compacted to beyond the critical pressure for grain crushing (marked by the arrows). Data which were shown in Figure 3 are connected by dashed lines. Note the change in pressure sensitivity and the drastic decrease in permeability (especially in the Boise sandstone) which accompanied the grain crushing process.

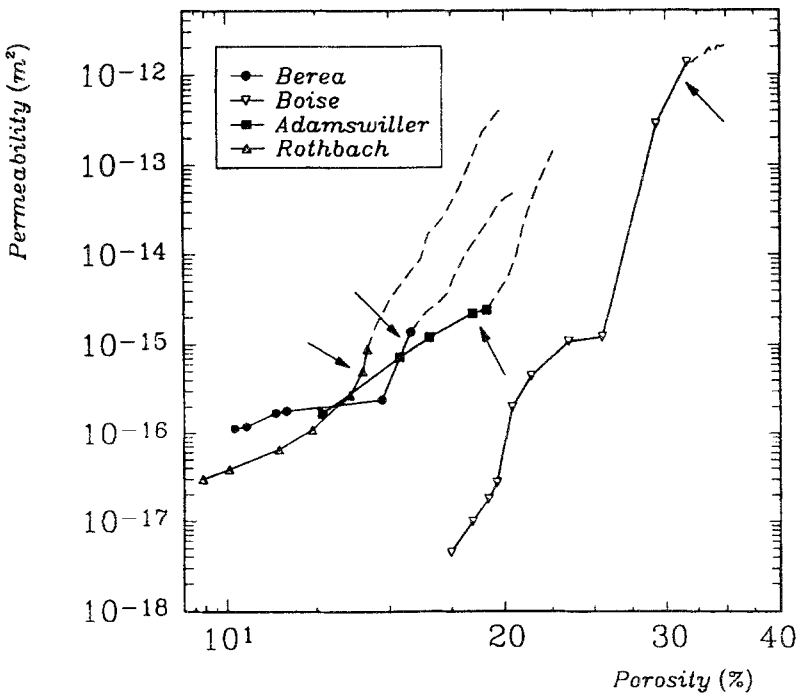

Figure 6
Permeability as a function of porosity in 4 sandstones compacted to beyond the critical pressure for grain crushing (marked by the arrows). Data which were shown in Figure 4 are connected by dashed lines.

much smaller, but there were evident changes in the slopes near the critical pressure. It is worth noting that both sandstones have already undergone a large permeability loss in the region below the critical pressure (almost two orders of magnitude). The maximum permeability decrease that we observed over the whole pressure range is six orders of magnitude for Boise sandstone.

We expect that two mechanisms are operative simultaneously with opposite effects on the permeability evolution. At the onset of grain crushing, the solid framework of the rock is weakened, resulting in a partial loss in cohesion and fragmentation of grains. The micromechanics has been elucidated by a thorough examination of the microstructures of the deformed samples (ZHANG *et al.*, 1990a). The pore space collapses, and more importantly debris fills the pores and clogs the throats where fluid has to flow through. Such features are very often found in samples tested at effective pressures above the critical pressure. This process induces a dramatic decrease in permeability for this simple reason that the mean cross-sectional area of the effective pore throats has been reduced significantly. The second physical process is that simultaneously extensile cracking at the grain scale opens

many new paths for the fluid to flow through the rock, resulting in a decrease in the hydraulic tortuosity which will produce an enhancement of the permeability. The net effect which was observed in our experiments is a permeability reduction: this tells us that the first mechanism was dominant. However, the transition towards a weaker permeability-porosity dependence in the grain crushing regime demonstrates that the second mechanism was operative as well and also played a significant role.

Our data also suggest that the decrease in permeability induced by pore collapse is smaller for rocks with a significant clay content than for clay-free rocks. This must be confirmed on a larger set of rocks. It is well documented that clays modify significantly the hydraulic properties of clay-rich rocks due to physico-chemical interactions with water (e.g., DEY, 1986). Our data suggest that clays also result in the drastic change in hydromechanical behavior at the onset of grain crushing to be more gradual.

From Figures 5 and 6 it can be seen that after the dramatic drop in permeability at the onset of grain crushing both the pressure sensitivity and porosity sensitivity decreased while grain crushing was in progress. For example, in Berea sandstone there was a transition from an exponent $\alpha = 15$ before the onset of grain crushing towards a weaker dependence with $\alpha = 2.0$ in the grain crushing regime. Boise sandstone presents a more complicated behavior in the grain crushing regime with a second stage of accelerated permeability reduction which may be associated with a further pore collapse in the compacted rock sample. Overall, the permeability change in the grain crushing regime displays a complex pattern both with respect to pressure and porosity, and it is unrealistic to fit the data with either equation (1) or (2).

Permeability as a Function of Pressure and Porosity in Rocks and Fractures

Our new data on five porous sandstones highlight several characteristics of permeability as a function of pressure and porosity. First, if the compaction mechanism involves grain rearrangement without grain crushing, then the data are in reasonable agreement with the empirical relations (1) and (2). Second, the dramatic decrease of up to 3 orders of magnitude in permeability is associated with the onset of grain crushing. Third, the porosity sensitivity exponent α and the pressure sensitivity coefficient γ have a wide range of values.

Our data are for sandstones with porosities greater than 10%. To further understand the pressure and porosity sensitivity of permeability, we have compiled experimental data published in the literature (Table 3). We compare the data for sandstones and crystalline rocks of relatively low porosity to investigate the effect of porosity and crack closure. To analyze the effect of lithification and cementation, we compare our data with data for unconsolidated sand and fault gouge. We also compare the effect of chemical compaction mechanisms with mechanical

Table 3

Compilation of published data on the pressure and porosity sensitivity of permeability for different rocks

Reference	Rock type	α	γ, 10^{-2} MPa^{-1}	σ^*, MPa
Mechanical Compaction				
	High porosity rocks			
This study	sandstones	4.6–25.4	0.66–1.2	80.5–151
YALE (1984)	sandstones	1.86–12.6	0.14–2.0	50.0–714
NELSON and ANDERSON (1992)	ash flow tuffs	3–10.6	*	*
	Low porosity rocks			
YALE (1984)	tight sandstones	5–25	3.8–6.3	15.9–26.3
BRACE *et al.* (1968)	Westerly granite	3	3.3	30.6
BERNABÉ (1986)	Chelmsford granite	*	2.9	34.6
	Barre granite	*	2.3	42.7
FISCHER and PATERSON (1992)	Carrara marble	*	4.7	21.3
HUENGES and WILL (1989)	Urach gneiss	*	4.9	20.4
MORROW *et al.* (1994)	gneiss [Kola]	*	3.2	31.2
	basalt [Kola]	*	10.2	9.8
	amphibolite [KTB]	*	5.8–11.0	9.1–17.2
	Granular material			
ZOBACK and BYERLEE (1976)	Ottawa sand	1.11	0.18	568
	Fault gouge			
MORROW *et al.* (1984)	clay-free gouge	*	0.45–1.4	70.6–222
	clay gouge	*	1.2–5.5	18.2–81.3
	Fractured rocks			
KRANZ *et al.* (1979)	jointed Barre granite	≈ 3	7.8–9.2	10.9–12.8
RAVEN and GALE (1985)	natural rock joint	*	10.9	9.1
Chemical Compaction				
BERNABÉ *et al.* (1982)	hot-pressed calcite	3–10.7	*	*
ZHANG *et al.* (1994)	hot-pressed calcite	3–14	*	*
BOURBIÉ and ZINSZNER (1985)	Fontainebleau sandstone	3–7.3	*	*

compaction, and finally the effect of preexisting fractures is analyzed by comparing the intact rock and fractured rock permeabilities.

Mechanical Compaction of Intact Rock

We first consider permeability data for intact rocks. YALE (1984) presented in his doctoral thesis data for sandstones with porosities ranging from 2% to 27%. The pressure range was relatively narrow and thus the hydrostats for his sandstones with porosities greater than 7% show typical type-II behavior. We determined the coefficients α and γ for YALE's (1984) high porosity samples, which together with our sandstone data are plotted as solid symbols in Figure 8. The two sets of data are consistent in that both coefficients span a wide spectrum of values, with γ ranging from 0.001/MPa to 0.020/MPa and α ranging from 1.9 to 25. There is a

positive correlation between α and γ which can be explained by noting that equations (1) and (2) imply the following relationship between the two coefficients:

$$\gamma = -\frac{\alpha}{\Phi}\frac{d\Phi}{dP} = \alpha\beta_\phi \tag{3}$$

where β_ϕ denotes the pore compressibility (which has to be positive). A high γ/α ratio results from a relatively compressible pore space. The data for porous sandstones in Figure 8 can be bracketed by two linear boundaries corresponding to $\beta_\phi = 4.4 \times 10^{-4}$/MPa and 3.3×10^{-3}/MPa, respectively.

In low porosity crystalline rocks, permeability as a function of pressure has been intensively studied. Most published data show an approximately exponential relation while the relatively thin cracks are closed during hydrostatic loading for the first 100 MPa or so, after which the permeability becomes less sensitive to pressure (see Figure 1). We estimate the pressure sensitivity coefficients for the initial crack closure, and therefore the values for granite, marble and gneiss compiled in Table 3 represent upper bounds on the pressure sensitivity. The tight rocks have a coefficient $\gamma > 0.02$/MPa, about an order of magnitude greater than those of the porous sandstones.

Little data exist for permeability as a function of porosity partly because the relatively small porosity change due to crack closure is hard to resolve. For Westerly granite we can indirectly infer the value of α from the permeability data of BRACE *et al.* (1968) which show a correlation with the formation factor F in the form $K \propto F^{-1.5}$, and the electrical resistivity data of BRACE *et al.* (1965) which approximately follow Archie's law in the form $F \propto \Phi^{-2}$. Therefore one expects $K \propto \Phi^3$ and $\alpha \cong 3$ for Westerly granite. We also estimated the coefficients α and γ of several tight sandstones ($\Phi < 7\%$) from YALE's (1984) data. As can be seen from Table 3, the pressure sensitivity coefficients of the tight sandstones are comparable to the granites and the gneiss, and they are significantly greater than those for the porous sandstones. However, the porosity sensitivity exponents span a range comparable to that of the porous sandstones. Consequently, when we consider the γ/α ratio (Figure 7), Westerly granite and YALE's (1984) tight sandstones fall into a group (the open symbols) with values higher than the porous sandstones.

The high γ/α ratio in low porosity rocks is probably a manifestation of crack closure processes. According to equation (3), the ratio corresponds to the pore compressibility which can be shown to be inversely proportional to the crack aspect ratio. For example, if we follow WALSH's (1965) analysis of the closure of a penny-shaped crack (with aspect ratio ε) embedded in an elastic medium (with compressibility β and Poisson ratio ν), we obtain the following expression for the pore compressibility:

$$\beta_\phi = \beta\left[\frac{4}{3\pi}\frac{(1-\nu^2)}{(1-2\nu)\varepsilon} - 1\right]. \tag{4}$$

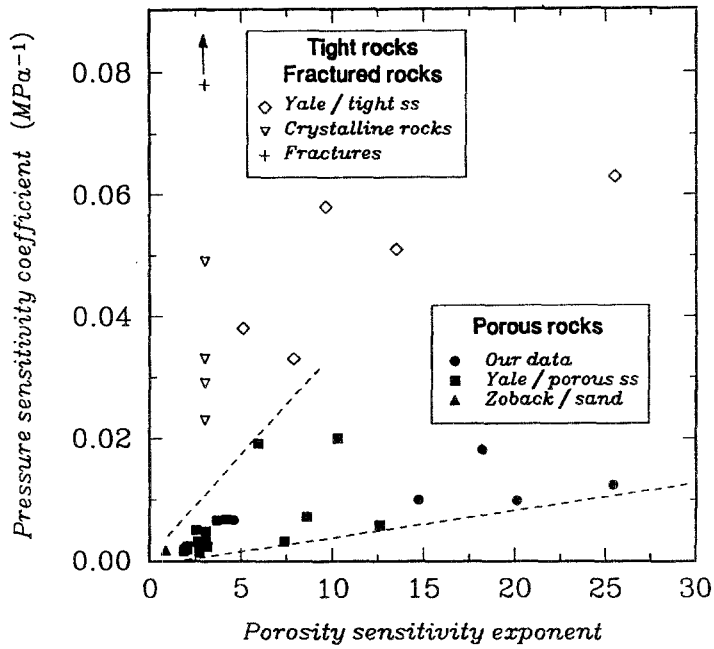

Figure 7

Correlation between the pressure sensitivity coefficient γ and the porosity sensitivity exponent α for sandstones, sand, crystalline rocks and jointed rocks (see compilation in Table 3). It is shown in the text that the ratio γ/α represents the pore compressibility. The data can be separated into two distinct groups: (i) low porosity (crystalline and clastic) rocks and rock fractures which have high ratios of γ/α, indicative of a relatively compressible pore space; (ii) porous sandstones and unconsolidated sand with relatively low ratios of γ/α, indicative of a relatively stiff pore space.

From Table 3 Westerly granite has $\beta_\phi = \gamma/\alpha = 0.011$/MPa and if we assume representative values for the elastic moduli ($\beta = 0.02\ \text{GPa}^{-1}$ and $\nu = 0.25$), then according to equation (4), the aspect ratio $\varepsilon = 1.4 \times 10^{-3}$, in reasonable agreement with estimates from mechanical (BRACE, 1965) and microstructural (HADLEY, 1976) measurements. Altogether the tight rock data shown in Figure 7 correspond to $\beta_\phi = \gamma/\alpha > 3.3 \times 10^{-3}$/MPa, implying that the relatively thin cracks in the low porosity rocks are such that their aspect ratios $\varepsilon < 5 \times 10^{-3}$.

The data compiled here highlight two important aspects of permeability in intact rock which have received little attention before. First, the permeability of a tight rock has a pressure sensitivity significantly higher than that of a porous rock. Second, the ratio of the pressure sensitivity to the porosity sensitivity reflects the compressibility of the pore space, and this ratio is also significantly higher in a tight rock. As we have emphasized in this study, the differences are related to the compaction mechanisms. To date the conclusions are primarily based on phenomenological observations, and it is desirable to have a deeper understanding of

the microphysical basis for permeability evolution as a function of porosity and stress.

In a porous sandstone, the mechanisms involve inelastic and frictional processes which are relatively difficult to model. In contrast, crack closure in tight rocks is elastic and important advances have been made in the modeling of the pressure dependence of permeability. For example, WALSH (1981) considered the Hertzian contact of rough fracture surfaces and the associated hydraulic transport process. According to his analysis, if the crack surfaces have a mean aperture a_0 (at the reference pressure P_0) and a root mean square roughness h, then the pressure sensitivity of permeability is characterized by the following equation:

$$\left[\frac{K}{K_0}\right]^{1/3} = 1 - \frac{\sqrt{2}h}{a_0} \ln\left(\frac{P}{P_0}\right). \tag{5}$$

Data for Westerly granite obtained by MORROW *et al.* (1986) are in reasonable agreement with WALSH's (1981) model. To establish possible connections between the exponential equation (1) and WALSH's (1981) model, we calculated the normalized permeability K/K_0 as a function of the normalized pressure p/p_0 according to the empirical relation (1), and then we plotted $(K/K_0)^{1/3}$, the cubic root of the calculated permeability as a function of the logarithm of the normalized pressure (Figure 8). If the two models are consistent, then the plot should be approximately linear following equation (5). It can be seen from Figure 8 that each of the plots is approximately linear within a characteristic pressure range of about an order of magnitude. For Westerly granite (with $\gamma = 0.033$/MPa), the plot is approximately linear at effective pressures between 20 MPa and 200 MPa with a slope of about 0.6. Within this pressure range, equations (2) and (5) predict similar pressure dependence for the permeability of Westerly granite. In comparison, the data of MORROW *et al.* (1986) were for effective pressures ranging between 10 MPa and 90 MPa, and when fitted to equation (5), their data fall on lines with the slope between 0.4 to 0.6. If we take the slope to be 0.6, then according to equation (5) the normalized roughness $h/a_0 = 0.18$, which is a reasonable estimate (WALSH, 1981).

Equation (1) has the advantage of being mathematically simple, but unlike equation (5) it is a phenomenological relation without any micromechanical basis. The comparison here shows that for a given rock type, there exists a pressure range over which the two relations are approximately equivalent and hence the exponential relation can be adopted for mathematical convenience. Although WALSH's (1981) analysis was originally for fracture closure, it seems that his model may also apply to high porosity rocks since they also show the exponential type of pressure dependence. Indeed, BERNABÉ (1991) argued that his compilation of sandstone data is in agreement with a Hertzian contact model. His analysis also highlights an important limitation of this type of contact model in that it is very sensitive to the

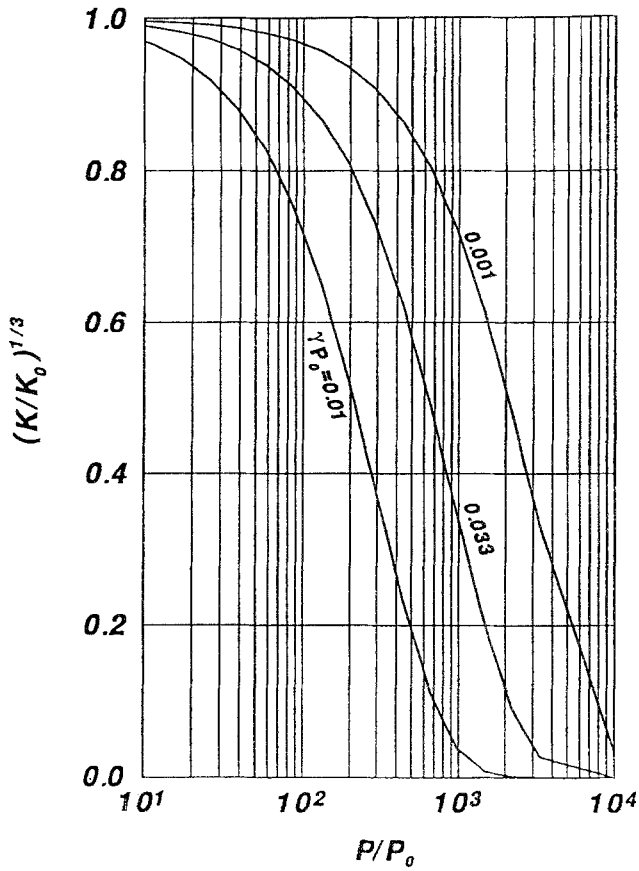

Figure 8

Comparison of two relations for the pressure dependence of permeability. The first is the empirical exponential relation given by equation (1) in the text. The second relation is based on WALSH's (1981) micromechanical model for elastic contact of rough surfaces, given by equation (5) in the text. The permeability was first calculated according to the exponential relation, and its cubic root is plotted versus the effective pressure (in log scale). According to equation (5) such a plot should be linear. It can be seen that for a fixed value of the parameter γP_0, there exists a pressure range of about 100 MPa over which the plot is linear. Within this pressure range, the two relations can be considered as approximately equivalent.

statistics of the asperity height on the rough contact surfaces. Following his earlier analysis (WALSH and GROSENBAUGH, 1979), WALSH (1981) assumed a negative exponential distribution which may not be an appropriate statistical characterization of the pore space of Westerly granite (WONG *et al.*, 1989). Making somewhat different assumptions about the roughness, BERNABÉ (1991) came up with a pressure dependence which is quite different from equation (5), with the right-hand side given by $(K/K_0)^{1/4}$ instead.

Compaction of Unconsolidated Material and Closure of Fracture

In many tectonic settings (e.g., accretionary prisms, sedimentary basins and fault gouge zones in seismogenic systems), one also has to deal with the permeability of unconsolidated materials. Little data exist on the permeability of soil and sediment at elevated pressures. A relatively complete set of data was presented by ZOBACK and BYERLEE (1976) for Ottawa sand at effective pressures up to 300 MPa, beyond the onset of grain crushing. Focusing on their data for hydrostatic compaction before the onset of grain crushing, we determined the pressure and porosity sensitivities to be $\alpha = 1.11$ and $\gamma = 1.8 \times 10^{-3}$/MPa respectively (Table 3). These values are comparable to the low-end values of the porous sandstones (Figure 7).

Permeability measurements have also been made on fault gouge subjected to pressure and shear loading. The most comprehensive set of data was presented by MORROW *et al.* (1984), but since it was difficult to determine the porosity change, no information on the porosity sensitivity was available. They concluded that the permeability was principally controlled by the mean pressure, and the pressure sensitivity coefficients we determined from their data are included in Table 3. The clay-free gouges have γ values which are comparable to the porous sandstones but lower than the tight rocks. For these samples, MORROW *et al.* (1984) observed a correlation between the pressure dependence of permeability and the extent of grain crushing. In contrast, the clay-rich gouges have γ values which are comparable to Westerly granite and other low porosity rocks. The strong pressure dependence is probably a manifestation of the relatively high compressibility of clay (LAMBE and WHITMAN, 1969). However, it is difficult to interpret the data further in the absence of information on the porosity sensitivity. It should also be noted that permeability anisotropy may develop as a result of nonhydrostatic stress (e.g., ZOBACK and BYERLEE, 1976; BRUNO *et al.*, 1991) and shear localization (e.g., ARCH and MALTMANN, 1990) which can strongly influence the hydraulic transport processes in a fault zone (RICE, 1992).

Since fractures exist on all scales in the crust, it is important to study the permeability change in relation to the closure of preexisting fractures. There have been many studies of the pressure dependence of the permeability of rock joints, both *in situ* and in the laboratory (see review by RAVEN and GALE, 1985). The data are consistent in that they show the highest pressure sensitivity, with γ values greater than those of intact rocks as well as unconsolidated materials (Table 3). In the presence of preexisting fractures, there are two separate sets of porosities (corresponding to the fracture opening and the matrix porosity of the country rock) and therefore the porosity sensitivity of permeability is not well defined. However, if we focus on the pore space of the fracture opening, then the porosity sensitivity exponent $\alpha \approx 3$ since the flow rate through a fracture is related to the opening by the so called "cubic law." A representative value for α and γ for fractures is marked

by a cross in Figure 7. It can be seen that overall they have the highest ratios of γ/α, which is not unexpected since fractures are expected to be elastically more compliant than intact rocks (e.g., WALSH and GROSENBAUGH, 1979).

Cementation and Healing Processes

To date, we have focused on mechanical compaction by brittle processes. In diagenetic and tectonic settings, significant permeability change may also be induced by chemical compaction processes (such as cementation, pressure solution and solution-precipitation) under a hydrothermal condition. The temporal evolution of permeability in such cases is expected to be complex, since the evolution of the pore space is controlled by the kinetics of the chemical processes, diffusive mass transfer, crystal plasticity as well as the fluid transport. Nevertheless, a number of recent laboratory studies under controlled conditions suggest that in chemical compaction processes, permeability is related to porosity in a relatively simple manner.

The first systematic study was by BERNABÉ *et al.* (1982), who measured the permeability of a suite of calcite aggregates (with porosities ranging from 6% to 20% prepared by hot-pressing. They observed two distinct regimes with the permeability showing qualitatively different porosity sensitivity. At porosities larger than about 11%, the permeability data are in good agreement with the power law (equation (2)), with an exponent $\alpha \approx 3$. In contrast, at porosities smaller than 11% the porosity sensitivity was observed to increase with decreasing porosity and it is not possible to fit the data with a single exponent. We estimated that the maximum slope for their data to correspond to $\alpha \approx 10$ (Table 3). ZHANG *et al.* (1994) recently conducted *in situ* measurements of permeability of calcite aggregates inside an internally heated pressure vessel during hot-pressing. They also observed $\alpha \approx 3$ above a crossover porosity ($=7\%$, lower than that 11% value of BERNABÉ *et al.*, 1982), and the exponent was observed to attain a value as high as 14 at porosities below the crossover.

Similar permeability-porosity systematics in Fontainebleau sandstone were also reported by BOURBIÉ and ZINSZNER (1985). This sandstone is monominerallic and does not show much variability in grain size or sorting. However, it has a wide variability in porosity due to different degrees of silicification during its diagenetic evolution. Gas permeability measurements of a suite of Fontainebleau sandstone (with porosities ranging from 3% to 28%) were conducted under room conditions. The crossover porosity was about 9%, above which the permeability increased with porosity in accordance with a power law with $\alpha = 3.05$. Below the crossover, the porosity sensitivity exponent increased to a value up to 7.3.

The qualitative differences between the two regimes above and below the crossover porosity suggest that two distinct mechanisms are operative. A theoretical model must account for the dramatic decrease of permeability with compaction

below the crossover and the relatively constant value of $\alpha \approx 3$ for porosities above the crossover. In hot-pressed samples compacted below the crossover porosity, BERNABÉ *et al.* (1982) observed that tubular pores along grain edges had been pinched off and they attributed the dramatic decrease of permeability to connectivity loss in the pore space induced by this mechanism. We recently developed a network percolation model (ZHU *et al.*, 1993) to simulate this mechanism. Using pore size distribution from quantitative microstructural measurements and assuming that the overall loss of connectivity was linearly related to porosity reduction, we were able to model the effect of hot-pressing and cementation on the permeability of calcite aggregate (BERNABÉ *et al.*, 1982) and Fontainebleau sandstone (BOURBIÉ and ZINSZNER, 1985) and on the electrical conductivity of quartz aggregate (LOCKNER, 1990). The decrease in connectivity was simulated by randomly breaking off conducting bonds in a simple cubic network. In our model the permeability becomes vanishingly small at the percolation threshold.

Above the crossover porosity, microstructural observations have indicated that porosity reduction is primarily by shrinkage of the individual pores without any significant changes in the overall connectivity. The porosity sensitivity for such a mechanism was considered by WONG *et al.* (1984), who demonstrated that if conducting elements are randomly selected and the pore sizes are allowed to shrink by a factor x, then the permeability has a power-law dependence on the porosity. In their model, the shrinkage factor x is fixed and it is a measure of the skewness of the pore size distribution. The smaller x is, the more skewed is the distribution and the larger is the porosity sensitivity exponent α. In particular, the exponent is about 3 for a shrinkage factor $x = 0.5$. While this model explains how the skewness of pore size distribution influences porosity sensitivity of permeability, it does not explain why the diagenetic and deformation mechanisms act in such a peculiar manner that the spatial location of pore shrinkage is random and yet the shrinkage factor is deterministic. ZHU *et al.* (1993) recently show that it is not necessary to incorporate this apparently contradictory feature in the pore shrinkage model. In our modified model, the shrinkage factor is not arbitrarily fixed but rather is a random number between 0 and 1. Simulations of the permeability evolution in a simple cubic network consistently show a porosity sensitivity of $\alpha \approx 3$, in good agreement with data for hot-pressed calcite and Fontainebleau sandstone at porosities above the crossover. Details of the network percolation model will be presented in a future publication.

Can a similar analysis be applied to mechanical compaction processes? As Table 3 shows, mechanical compaction of porous aggregates is usually associated with relatively high porosity sensitivity exponent α. Such high exponents for the permeability-porosity evolution correspond to a situation where pocket-like pores contribute much to the porosity and little to the permeability. This is in agreement with recent numerical simulations by DAVID (1991) who found an exponent $\alpha = 2$ for a constant pore channel geometry in his network model, and exponents ranging from

3.5 to 23 in situations where the distributions of pore channel aspect ratio are log-normal. Our microstructural observations indicate that the pore geometry of the mechanically compacted sandstone samples is highly heterogeneous, with both large equant pores and micropores associated with clays or altered feldspars, as well as intragranular and grain boundary microcracks. If the compaction involves appreciable grain rotation and boundary sliding, it is plausible that such processes modify the permeability more efficiently (e.g., by closing the pore throats) than it reduces the porosity. We are employing the network model with microstructural measurements to analyze mechanical compaction of porous aggregates, and the detailed results will be presented in a future publication.

DAVID (1993) also showed that in many cases fluid flow is likely to occur preferentially in critical paths controlled by the spatial distribution of large pore channels. Consequently, the overall permeability is controlled by a relatively small fraction of the interconnected pore space, and therefore variation in bulk porosity may not be the only microstructural parameter influencing permeability evolution. However, many theoretical models appeal to such a correlation between permeability and bulk porosity: the broad range of porosity sensitivity shown by common geologic materials for different compaction mechanisms should be taken into account in any theoretical models for the development of pore pressure excess in the crust.

Development of Pore Pressure Excess in Seismogenic System

While it is well documented that the magnitude of permeability in common geologic materials spans more than 10 orders of magnitude, it is little appreciated that both the pressure sensitivity and porosity sensitivity of permeability show significant variations in the laboratory (Table 3 and Figure 7). In light of the laboratory observations, we assess their implications on the development of crustal pore pressure, focusing on two recent models which explicitly assumed permeability to be a variable sensitively dependent on pressure or porosity.

We first consider the model formulated by RICE (1992) for the generation and maintenance of pore pressure excess in a seismogenic system such as the San Andreas Fault. To generate the overpressure, RICE (1992) appealed to the continuous influx q of fluid from the "ductile root" of the fault zone and to maintain the pore pressure within the fault zone at close to lithostatic level, he assumed the permeability to be a rapidly diminishing function of the effective normal stress $\bar{\sigma}$. In particular, he assumed an exponential dependence of the form:

$$K = K_0 \exp(-\bar{\sigma}/\sigma^*) \tag{6a}$$

and he provided numerical results for $\sigma^* = 5$ MPa. Under hydrostatic loading, the characteristic stress σ^* is equal to the reciprocal of the pressure sensitivity co-

efficient given in equation (1) above:

$$\sigma^* = 1/\gamma. \tag{6b}$$

According to RICE's (1992) one-dimensional steady-state flow model, the pore pressure distribution can be derived as follows. If the densities of the saturated rock mass and the fluid are denoted by ρ_r and ρ_f, respectively and the fluid viscosity by η, then the pore pressure distribution as a function of depth z (assumed to be positive downward) is given by

$$P(z) = \rho_f g z + \sigma^* \ln\{1 + \xi[\exp((\rho_r - \rho_f)gz/\sigma^*) - 1]\} \tag{7a}$$

with the normalized flux given by

$$\xi = \frac{q\eta}{(\rho_r - \rho_f)gK_0}. \tag{7b}$$

The first term represents the hydrostatic contribution, and the second term represents the pore pressure excess induced by the fluid influx. Figure 9 illustrates

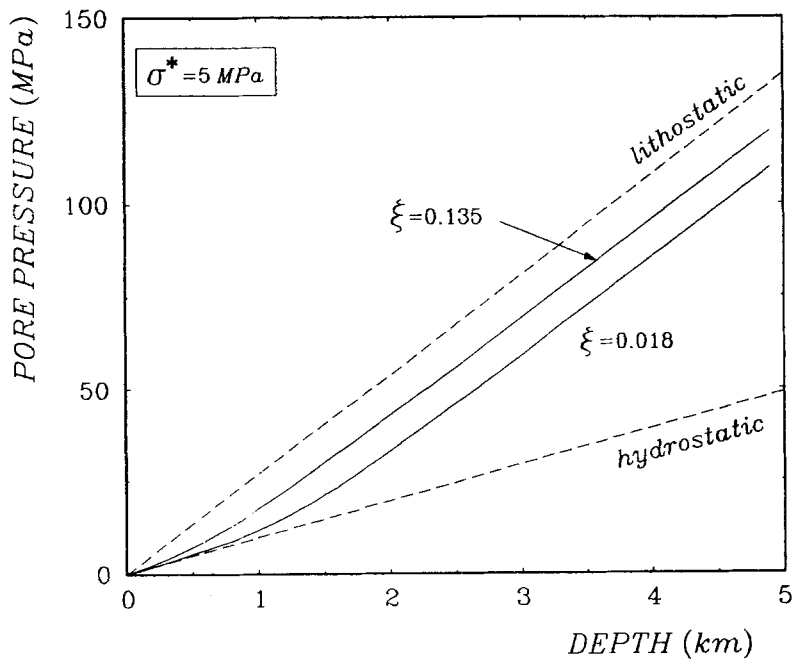

Figure 9

Pore pressure as a function of depth calculated using equation (7a) according to RICE's (1992) model for the development of overpressure in a seismogenic system. Two different values of ξ (normalized influx of fluid from below the seismogenic layer) were used, and a relatively high pressure sensitivity of permeability (corresponding to $\sigma^* = 1/\gamma = 5$ MPa) was assumed. Note that beyond about 1 km, the pore pressure differes from the lithostatic value by fixed small amounts of 10 and 20 MPa, respectively.

the pore pressure distribution for two different values of ξ (0.135 and 0.018). Although the pore pressure is constrained by the boundary condition to be hydrostatic near the surface, the pore pressure excess builds up rapidly so that the hydraulic gradient approaches lithostatic at depths below 1 km or so. Below this transition depth, the effective normal stress $\bar{\sigma}$ attains asymptotic values of 10 MPa and 20 MPa, respectively. In computing the results for Figure 9, the densities are taken to be $\rho_r = 2700$ kg/m^3 and $\rho_f = 1000$ kg/m^3, and following RICE (1992) we fix $\sigma^* = 5$ MPa. This value is lower than most of the laboratory measurements, and our compilation in Table 3 shows that porous aggregates can have values of σ^* one or two orders of magnitude higher.

The influence of σ^* ($= 1/\gamma$) on the pore pressure development can be illustrated by focusing on the maximum pore pressure which is attained at the bottom of the seismogenic zone. If we denote the seismogenic thickness by H and introduce the

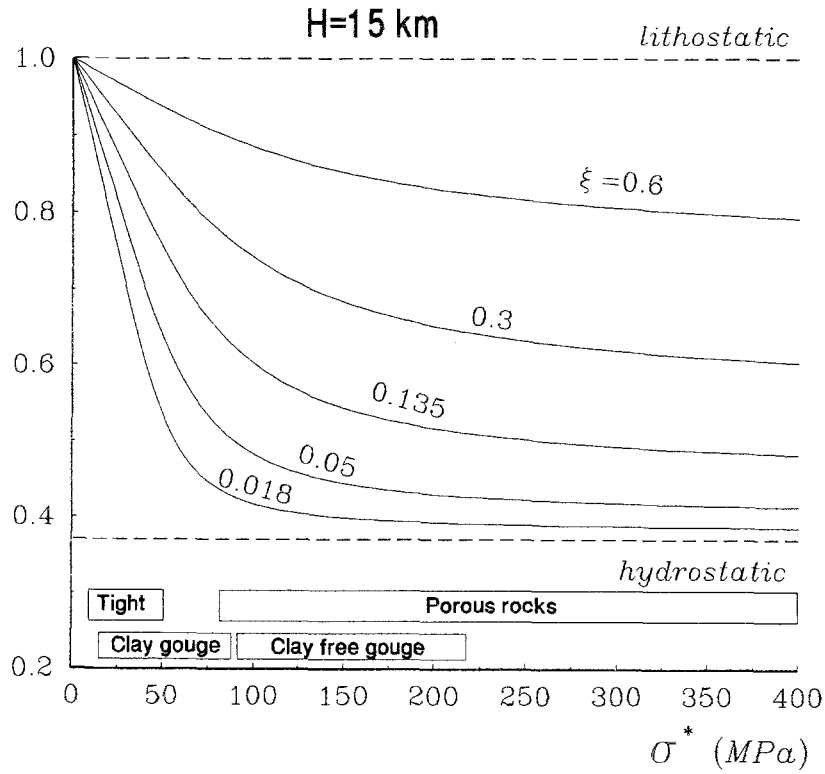

Figure 10

The Hubbert-Rubey pore pressure ratio λ (at the base of the seismogenic layer) as a function of the reciprocal pressure sensitivity of permeability ($\sigma^* = 1/\gamma$) calculated according to equation (8). For a fixed amount of normalized fluid influx ξ, the pore pressure excess decreases rapidly with increasing σ^* (i.e., with decreasing pressure sensitivity of permeability). Ranges of values for σ^* in rocks and unconsolidated materials (compiled in Table 3) are also indicated.

Hubbert-Rubey pore pressure coefficient $\lambda = P(H)/\rho_r gH$, then from equation (7a) we can derive the following relation

$$\lambda = \frac{\rho_f}{\rho_r} + \frac{\sigma^*}{\rho_r gH} \ln\left\{1 + \xi\left[\exp\left(\frac{(\rho_r - \rho_f)gH}{\sigma^*}\right) - 1\right]\right\}. \tag{8}$$

Assuming a seismogenic thickness $H = 15$ km, we plot in Figure 10 the pore pressure coefficient λ at the base of the seismogenic zone as a function of σ^* for fixed values of ξ. For $\xi = 0.018$, if σ^* increases from 5 MPa (the value used in Figure 9) to 100 MPa, then the pore pressure would drop from near lithostatic ($\lambda = 0.94$) to near hydrostatic ($\lambda = 0.42$). Hence for $\sigma^* > 100$ MPa which is typical of porous aggregates, development of overpressure requires ξ to be greater than 0.6 or so, corresponding to a very significant influx of fluid from below the seismogenic zone. Taking the viscosity $\eta = 0.001$ Pa s and room-pressure permeability $K_0 = 10^{-15}$ m^2 (1 millidarcy), we can apply equation (7b) to estimate the fluid influx to be $q = 315$ mm/yr corresponding to $\xi = 0.6$. If we consider a fault zone of cross section 10 km × 100 m, this corresponds to a total discharge of as much as 3.15×10^5 m^3/yr. On the other hand, if we follow RICE (1992) to take $\sigma^* = 5$ MPa for low porosity crystalline rocks and rock joints, then near lithostatic pressure can be maintained even if ξ is as small as 0.02 (Figures 9 and 10). Since the room-pressure permeability would also be relatively low (on the order of 0.01 millidarcy, BRACE, 1980), equation (7b) implies the fluid influx $q \approx 0.1$ mm/yr, three orders of magnitude smaller than for porous aggregates.

A major unknown in RICE's (1992) model is the kinetics of the fluid influx. If this flux is fixed, then the pore pressure excess which can develop is a function of both the absolute value of permeability and its pressure sensitivity. Because they have low permeabilities and high pressure sensitivities, low porosity crystalline rocks and rock joints provide the most favorable conditions for the development of overpressure. On the other hand, porous rocks and unconsolidated materials require appreciable influx of fluid for RICE's (1992) mechanism to work. Because of their relatively low permeabilities, clay-rich gouges and shaly sandstones are expected to display intermediate behavior.

In an elegant analysis, RICE (1992) also demonstrated the possibility for fluid injection as vertically propagating pressure pulses into the seismogenic system. If an ambient pore pressure excess (such as shown in Figure 9) exists in the fault zone and if the permeability K and porosity Φ depend on the effective normal stress according to $K = F(\bar{\sigma})$ and $\rho_f \Phi = G(\bar{\sigma})$, respectively, then fluid pulses can propagate upward as solitary waves if the following inequality holds

$$\frac{F(\bar{\sigma}) - F(\bar{\sigma}_2)}{F(\bar{\sigma}_1) - F(\bar{\sigma}_2)} < \frac{G(\bar{\sigma}) - G(\bar{\sigma}_2)}{G(\bar{\sigma}_1) - G(\sigma_2)} \quad \text{for} \quad \bar{\sigma}_1 < \bar{\sigma} < \bar{\sigma}_2. \tag{9a}$$

In terms of the pressure sensitivity coefficient γ and the pore compressibility β_ϕ, the two functions F and G are given in the following forms: $F(\bar{\sigma}) = K_0 \exp(-\gamma\bar{\sigma})$ and

$G(\bar{\sigma}) = \rho_f \Phi_0 \exp(-\beta_\phi \bar{\sigma})$, respectively. Note that the effective normal stress is with respect to the reference level at which the permeability and porosity are given by K_0 and Φ_0, respectively. Substituting into the above inequality, we arrive at

$$\frac{X^\alpha - X_2^\alpha}{X_1^\alpha - X_2^\alpha} < \frac{X - X_2}{X_1 - X_2} \quad \text{for} \quad X_1 > X > X_2 \tag{9b}$$

with $X = \exp(-\beta_\phi \bar{\sigma})$, $X_1 = \exp(-\beta_\phi \bar{\sigma}_1)$ and $X_2 = \exp(-\beta_\phi \bar{\sigma}_2)$. It can be shown that equation (9b) holds if the following inequality is applicable:

$$\alpha = \frac{\gamma}{\beta_\phi} > 1. \tag{9c}$$

From Table 3, the lowest value for the porosity sensitivity coefficient α is 1.11 (determined by ZOBACK and BYERLEE (1976) for Ottawa sand), and therefore we conclude that the permeability and compressibility of most geologic materials are such that vertically propagating pressure pulses can occur in accordance with RICE's (1992) model.

Porosity Reduction and Crustal Pore Pressure Development

We next consider WALDER and NUR's (1984) model which is on the overall development of pore pressure excess in a crustal layer instead of a localized fault system. The overpressure is generated by a generic porosity reduction mechanism, the kinetics of which is characterized by a porosity reduction rate $\dot{\Phi}$. The pore compressibility is assumed to be constant, and the permeability depends on porosity according to a power law similar to equation (2) except that it has a cutoff at a porosity Φ_c corresponding to the percolation threshold:

$$K = K_0 \left(\frac{\Phi^\alpha - \Phi_c^\alpha}{\Phi_0^\alpha - \Phi_c^\alpha} \right). \tag{10}$$

Except for very small porosities close to the percolation threshold, equation (10) is almost identical to equation (2). If we define the coordinate system with the z axis pointing vertically downward, then for a given porosity reduction rate the development of pore pressure excess $P' = P - \rho_f g z$ is governed by the following diffusion equation

$$\frac{1}{c} \frac{\partial P'}{\partial t} = \nabla^2 P' + \frac{\nabla K}{K} \cdot \nabla P' + \frac{\eta}{K} \dot{\Phi} \tag{11}$$

where the hydraulic diffusivity is $c = K/[\eta \Phi(\beta_\phi + \beta_f)]$ and the compressibility of the fluid is denoted by β_f. In equation (11) we have retained the term $\nabla K/K \cdot \nabla P'$ which was neglected by WALDER and NUR (1984). If the porosity reduction mechanism is operative within a crustal layer of thickness H, then near lithostatic

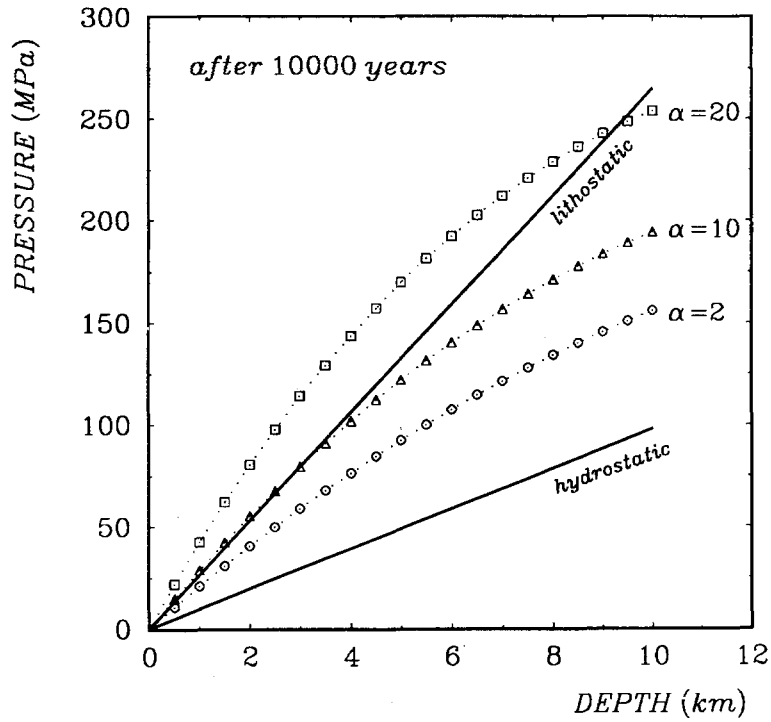

Figure 11
Pore pressure as a function of depth calculated using the finite-difference method according to WALDER and NUR's (1984) model for the development of overpressure in a crustal layer. The physical parameters are specified in the text, and compaction has endured for 10,000 years. Note that the generation of pore pressure excess is more efficient for increasing values of α (the porosity sensitivity exponent of permeability).

pressure can be generated and maintained if the following condition holds

$$\frac{\eta \dot{\Phi} H}{(\rho_r - \rho_f) g K} \gg 1. \tag{12}$$

The development of overpressure was illustrated by WALDER and NUR (1984) with numerical simulations for $\alpha = 2$ in equation (10) and with the porosity production rate $\dot{\Phi}$ ranging from 10^{-7}/s to 5×10^{-16}/s.

Our compilation in Table 3 shows that the mechanical compaction of unconsolidated materials and chemical compaction process has relatively low values of α, whereas higher porosity sensitivity is associated with the mechanical compaction of rocks in general. It is probably unrealistic to expect the chemical compaction processes to be completely decoupled from mechanical compaction in tectonic settings, and therefore the porosity sensitivity of permeability should be greater than that which is characterized by $\alpha = 2$. To investigate the influence of α on the

pore pressure development, we used the finite-difference method to solve the diffusion equation (11) for different values of α, the results of which are shown in Figure 11. Following WALDER and NUR (1984), we consider the one-dimensional transient flow problem with initially hydrostatic conditions and boundary conditions such that the pore pressure is hydrostatic at the surface ($z = 0$) and the lower surface ($z = h = 10$ km) is impermeable. The porosities at nominal condition and percolation threshold are $\Phi_0 = 0.2\%$ and $\Phi_c = 0.02\%$, and the nominal permeability is $K_0 = 10^{-19}$ m^2. The pore and fluid compressibilities are respectively $\beta_\phi = 10^{-11}$ Pa^{-1} and $\beta_f = 2 \times 10^{-10}$ Pa^{-1}, the fluid viscosity is $\eta = 2 \times 10^{-4}$ Pa s, and the porosity reduction rate is $\dot{\Phi} = 5 \times 10^{-16}$/s. The parameters are chosen such that for a relatively low porosity sensitivity of $\alpha = 2$, it is not possible to attain lithostatic values even after the porosity reduction mechanism has been operative for 10,000 years. However, if a coupled process involving mechanical and chemical compaction were to operate such that $\alpha \geq 10$, then lithostatic pore pressure can be generated and maintained over the same duration (Figure 11). The computations show superlithostatic pore pressure for $\alpha = 20$, but in reality dissipation by hydraulic fracturing will occur before such pore pressure excesses can build up (NUR and WALDER, 1992).

In this type of model, the major uncertainty is in relation to the kinetics of the compaction processes (e.g., GAVRILENKO and GUEGUEN, 1993). Further systematic studies on various healing and sealing processes will be very useful in placing constraints on the porosity reduction rate $\dot{\Phi}$. It should be noted that "shear compaction" processes have recently been proposed to be responsible for the generation of pore pressure excess in the San Andreas fault system (e.g., BLANPIED *et al.*, 1992). While the kinetics of such processes remain rather unspecific, the development of pore pressure excess in such a compaction model is expected to show dependence on the porosity sensitivity of permeability similar to that which is illustrated in Figure 11.

Acknowledgments

We thank Steven Cox and Dan Karig for their reviews. We have benefited from discussions with Yves Bernabé, Dan Davis, Carolyn Morrow and Dave Olgaard. This research was partially supported by the U.S. Geological Survey under grant 143493G2279 and NATO under grant CRG910927. The first author was also supported by Elf Aquitaine and the French Ministère des Affaires Etrangères on a postdoctoral fellowship during his stay at Stony Brook.

REFERENCES

ARCH, J., and MALTMAN, A. (1990), *Anisotropic Permeability and Tortuosity in Deformed Wet Sediments*, J. Geophys. Res. *95*, 9035–9045.

BANGS, N., WESTBROOK, G. K., LADD, J. W., and BUHL, P. (1990), *Seismic Velocities from the Barbados Ridge Complex and Indications of High Pore Pressures in an Accretionary Complex*, J. Geophys. Res. *95*, 8767–8782.

BERNABÉ, Y. (1986), *The Effective Pressure Law for Permeability in Chelmsford Granite and Barre Granite*, Int. J. Rock Mech. Min. Sci and Geomech. Abst. *23*, 267–275.

BERNABÉ, Y. (1987), *A Wide Range Permeameter for Use in Rock Physics*, Int. J. Rock Mech. Min. Sci. and Geomech. Abst. *24*, 309–315.

BERNABÉ, Y. (1991), *Pore Geometry and Pressure Dependence of the Transport Properties in Sandstones*, Geophys. *56*, 436–446.

BERNABÉ, Y., BRACE, W. F., and EVANS, B. (1982), *Permeability, Porosity and Pore Geometry of Hot Pressed Calcite*, Mech. Mat. *1*, 173–183.

BLANPIED, M. L., LOCKNER, D. A., and BYERLEE, J. D. (1992), *An Earthquake Mechanism Based on Rapid Sealing of Fault*, Nature *358*, 574–576.

BOURBIÉ, T., and ZINZSNER, B. (1985), *Hydraulic and Acoustic Properties as a Function of Porosity in Fontainebleau Sandstone*, J. Geophys. Res. *90*, 11524–11532.

BRACE, W. F. (1965), *Some New Measurements of Linear Compressibility of Rocks*, J. Geophys. Res. *70*, 391–398.

BRACE, W. F. (1978a), *Volume Change During Fracture and Frictional Sliding: A Review*, Pure and Appl. Geophys. *116*, 603–614.

BRACE, W. F. (1978b), *A Note on Permeability Changes in Geologic Materials due to Stress*, Pure and Appl. Geophys. *116*, 627–633.

BRACE, W. F. (1980), *Permeability of Crystalline and Argillaceous Rocks*, Int. J. Rock Mech. Min. Sci. and Geomech. Abst. *17*, 241–251.

BRACE, W. F., ORANGE, A. S., and MADDEN, T. R. (1965), *The Effect of Pressure on the Electrical Resistivity of Water Saturated Crystalline Rocks*, J. Geophys. Res. *70*, 5669–5678.

BRACE, W. F., WALSH, J. B., and FRANGOS, W. T. (1968), *Permeability of Granite under High Pressure*, J. Geophys. Res. *73*, 2225–2236.

BREDEHOEFT, J. D., and HANSHAW, B. B. (1968), *On the Maintenance of Anomalous Fluid Pressures. I Thick Sedimentary Sequences*, Geol. Soc. Am. Bull. *79*, 1097–1106.

BREDEHOEFT, J. D., and NORTON, D. L., *The Role of Fluids in Crustal Processes* (National Academy Press 1990), 170 pp.

BRUNO, M. S., BOVBERG, C. A., and NAKAGAWA, F. M., *Anisotropic stress influence on the permeability of weakly-cemented sandstones*. In *Rock as a Multidisciplinary Science*, Proc. 32nd US Rock Mech. Symp. (ed. J. C. Roegiers) (Balkema 1991), pp. 375–383.

BYERLEE, J. (1990), *Friction, Overpressure and Fault Normal Compression*, Geophys. Res. Lett. *17*, 2109–2112.

BYRNE, T., and FISHER, D. (1990), *Evidence for a Weak and Overpressured Décollement beneath Sediment-dominated Accretionary Prisms*, J. Geophys. Res. *95*, 9081–9097.

COYNER, K. B. (1984), *Effect of Stress, Pore Pressure, and Pore Fluids on Bulk Strain, Velocity, and Permeability in Rocks*, Ph.D. thesis, Stanford University.

DAVID, C. (1991), *La perméabilité et la conductivité électrique des roches dans la croûte: Expériences en laboratoire et modèles théoriques*, Ph.D. thesis, Univ. Strasbourg, France.

DAVID, C. (1993), *Geometry of Flow Path for Fluid Transport in Rocks*, J. Geophys. Res. *98*, 12267–12278.

DAVID, C., and DAROT, M. (1989), Permeability and conductivity of sandstones. In Proc. Symp. *Rock at Great Depth* (eds. Maury, V., and Fourmaintraux, D.) (Balkema 1989) Vol. 1, pp. 203–209.

DAVIS, D. M., SUPPE, J., and DAHLEN, F. A. (1983), *Mechanics of Fold and Thrust Belts and Accretionary Wedges*, J. Geophys. Res. *88*, 1153–1172.

DEBSCHUTZ, W., KRUCKEL, U., and SCHOPPER, J. R. (1989), Effects of geostatic stress and pore pressure on the Klinkenberg permeability factor and other fluid flow parameters. In Proc. Symp. *Rock at Great Depth* (eds. Maury, V., and Fourmaintraux, D.) (Balkema 1989) Vol. 1 pp. 179–186.

DEY, T. N. (1986), *Permeability and Electrical Conductivity Changes due to Hydrostatic Stress Cycling of Berea and Muddy J Sandstone*, J. Geophys. Res. *91*, 763–766.

ETHERIDGE, M. A., WALL, V. J., COX, S. F., and VERNON, R. H. (1984), *High Fluid Pressures during Regional Metamorphism and Deformation: Implications for Mass Transport and Deformation Mechanisms*, J. Geophys. Res. *89*, 4344–4358.

FISCHER, G., and PATERSON, M. S., *Measurements of permeability and storage capacity in rocks during deformation at high temperature and pressure.* In *Fault Mechanics and Transport Properties of Rocks* (eds. Evans, B., and Wong, T.-f.) (Academic Press 1992) pp. 213–252.

FREEZE, R. A., and CHERRY, J. A., *Groundwater* (Prentice-Hall, NJ 1979) 604 pp.

FYFE, W. F., PRICE, N. J., and THOMPSON, A. B., *Fluids in the Earth's Crust* (Elsevier, NY 1978) 383 pp.

GAVRILENKO, P., and GUEGUEN, Y. (1993), *Fluid Overpressures and Pressure Solution in the Crust*, Tectonophys. *217*, 91–110.

HADLEY, K. (1976), *Comparison of Calculated and Observed Crack Densities and Seismic Velocities in Westerly Granite*, J. Geophys. Res. *81*, 3484–3494.

HUBBERT, M. K., and RUBEY, W. W. (1959), *Role of Fluid Pressure in the Mechanics of Overthrust Faulting, I. Mechanics of Fluid-filled Porous Solids and its Implications to Overthrust Faulting*, Geol. Soc. Am Bull. *70*, 115–166.

HUENGES, E., and WILL, G., *Permeability, bulk modulus and complex resistivity in crystalline rocks.* In *Fluid Movements, Element Transport and the Composition of the Deep Crust*, NATO ASI, C281 (Kluwer, Dordrecht 1989) pp. 361–375.

KARIG, D. E. (1990), *Experimental and observational constraints on the mechanical behavior in the toes of accretionary prisms.* In *Deformation Mechanisms, Rheology and Tectonics* (eds. Knipe, R. J., and Rutter, E. H.) Geol. Soc. Sp. Pub. *54*, 383–398.

KRANZ, R. L., FRANKEL, A. D., ENGELDER, T., and SCHOLZ, C. H. (1979), *The Permeability of Whole and Jointed Barre Granite*, Int. J. Roch Mech. Min. Sci. *16*, 225–235.

LACHENBRUCH, A. H., and SASS, J. H. (1980), *Heat Flow and Energetics of the San Andreas Fault Zone*, J. Geophys. Res. *85*, 6185–6222.

LACHENBRUCH, A. H., and SASS, J. H. (1992), *Heat Flow from Cajon Pass, Fault Strength, and Tectonic Implications*, J. Geophys. Res. *97*, 4995–5015.

LAMBE, T. W., and WHITMAN, R. V., *Soil Mechanics* (John Wiley, New York 1969) 553 pp.

LOCKNER, D. A. (1990), *Modeling of Brittle Failure and Comparisons to Laboratory Experiments*, Ph.D. thesis, MIT.

MOORE, J. C. (1989), *Tectonics and Hydrogeology of Accretionary Prisms: Role of the Décollement Zone*, J. Struct. Geol. *11*, 95–106.

MORROW, C., LOCKNER, D., HICKMAN, S., RUSANOV, M., and RÖCKEL, T. (1994), *Effects of Lithology and Depth on the Permeability of Core Samples from the Kola and KTB Drillholes*, J. Geophys. Res. *99*, 7263–7274.

MORROW, C. A., SHI, L. Q., and BYERLEE, J. D. (1984), *Permeability of Fault Gouge under Confining Pressure and Shear Stress*, J. Geophys. Res. *99*, 3193–3200.

MORROW, C. A., ZHANG, B., and BYERLEE, J. D. (1986), *Effective Pressure Law for Permeability of Westerly Granite under Cyclic Loading*, J. Geophys. Res. *91*, 3870–3876.

NELSON, P. H., and ANDERSON, L. A. (1992), *Physical Properties of Ash Flow Tuff from Yucca Mountain, Nevada*, J. Geophys. Res. *97*, 6823–6841.

NUR, A., and WALDER, J., *Hydraulic pulses in the earth's crust.* In *Fault Mechanics and Transport Properties of Rocks* (eds. Evans, B., and Wong, T.-f.) (Academic Press, San Diego 1992), pp. 461–474.

PRATT, H. R., BLACK, A. D., BRACE, W. F., and SWOLFS, H. (1977), *Elastic and Transport Properties of an in situ Jointed Granite*, Int. J. Rock Mech. Min. Sci. and Geomech. Abstr. *14*, 35–45.

RAVEN, K. G., and GALE, J. E. (1985), *Water Flow in a Natural Rock Fracture as a Function of Stress and Sample Size*, Int. J. Rock Mech. Min. Sci. *22*, 251–261.

RICE, J. R. (1992), *Fault stress states, pore pressure distributions, and the weakness of the San Andreas Fault.* In *Fault Mechanics and Transport Properties of Rocks* (eds. Evans, B., and Wong, T.-f.) (Academic Press 1992) pp. 475–503.

RIEPE, L., SACHS, W., and SCHOPPER, J. R. (1983), *Pressure Effects on Permeability*, 8th Eurp. Form. Eval. Symp. Trans., London, Paper B, 1–24.

TORGERSEN, T. (1991), *Crustal-scale Fluid Transport: Magnitude and Mechanisms*, Geophys. Res. Lett. *18*, 917–918.

TRIMMER, D., BONNER, B., HEARD, H. C., and DUBA, A. (1980), *Effect of Pressure and Stress on Water Transport in Intact and Fractured Gabbro and Granite*, J. Geophys. Res. *85*, 7059–7071.

VROLIJK, P., MYERS, G., and MOORE, J. C. (1988), *Warm Fluid Migration along Tectonic Melanges in the Kodiak Accretionary Complex, Alaska*, J. Geophys. Res. *93*, 10313–10324.

WALDER, J., and NUR, A. (1984), *Porosity Reduction and Crustal Pore Pressure Development*, J. Geophys. Res. *89*, 11539–11548.

WALSH, J. B. (1965), *The Effect of Cracks on the Compressibility of Rocks*, J. Geophys. Res. *70*, 381–389.

WALSH, J. B. (1981), *Effect of Pore Pressure and Confining Pressure on Fracture Permeability*, Int. J. Rock Mech. Min. Sci. *18*, 429–435.

WALSH, J. B., and GROSENBAUGH, M. A. (1979), *A New Model for Analyzing the Effect of Fractures on Compressibility*, J. Geophys. Res. *84*, 3532–3536.

WONG, P.-z., KOPLIK, J., and TOMANIC, J. P. (1984), *Conductivity and Permeability of Rocks*, Phys. Rev. *B 30*, 6606–6614.

WONG, T.-f., FREDRICH, J. T., and GWANMESIA, G. B. (1989), *Crack Aperture Statistics and Pore Space Fractal Geometry of Westerly Granite and Rutland Quartzite: Implications for an Elastic Contact Model of Rock Compressibility*, J. Geophys. Res. *94*, 10267–10278.

YALE, D. P. (1984), *Network Modelling of Flow, Storage and Deformation in Porous Rocks*, Ph.D. thesis, Stanford University, Calif.

ZHANG, J., WONG, T.-f., and DAVIS, D. M. (1990a), *Micromechanics of Pressure-induced Grain Crushing in Porous Rocks*, J. Geophys. Res. *95*, 341–352.

ZHANG, J., WONG, T.-f., and DAVIS, D. M., *High pressure embrittlement and shear-enhanced compaction in Berea sandstone: Acoustic emission measurement and microstructural observation.* In *Rock Mechanics Contributions and Challenges*, Proceedings of the 31st U.S. Rock Mechanics Symposium (eds. Hustrulid, W. A., and Johnson, G. A.) (Balkema 1990b) pp. 653–660.

ZHANG, J., DAVIS, D. M., and WONG, T.-f. (1993), *Failure modes on tuff samples from Leg 131 in the Nankai accretionary wedge.* In *Proceedings of the Ocean Drilling Program, Scientific Results, Vol. 131*, 275–281.

ZHANG, S., COX, S. F., and PATERSON, M. S. (1994), *Porosity and Permeability Evolution during Hot Isostatic Pressing of Calcite Aggregates*, J. Geophys. Res. in press.

ZHU, W., DAVID, C., and WONG, T.-f. (1993), *Permeability Reduction Induced by Pore Shrinkage and Connectivity Loss: Microstructural Observations and Percolation Modeling* (Abstract), Trans. Amer. Geophys. Union, EOS *74*, 293.

ZOBACK, M. D., and BYERLEE, J. D. (1975), *Permeability and Effective Stress*, Am. Assoc. Pet. Geol. Bull. *59*, 154–158.

ZOBACK, M. D., and BYERLEE, J. D. (1976), *Effect of High-pressure Deformation on Permeability of Ottawa Sand*, Am. Assoc. Pet. Geol. Bull. *60*, 1531–1542.

ZOBACK, M. D., ZOBACK, M. L., MOUNT, V. S., SUPPE, J., EATON, J. P., HEALY, J. H., OPPENHEIMER, D., REASENBERG, P., JONES, L., RALEIGH, C. B., WONG, I. G., SCOTTI, O., and WENTWORTH, C. (1987), *New Evidence on the State of Stress of the San Andreas Fault System*, Science *238*, 1105–1111.

(Received August 30, 1993, revised February 22, 1994, accepted April 21, 1994)